Influence of reinforcement on microstructure and mechanical response of a magnesium alloy

M. Jayamathy[1], S. Seshan[1], S. V. Kailas[1], K. Kumar[1] and T. S. Srivatsan[2,*]

[1]Department of Mechanical Engineering, Indian Institute of Science, Bangalore 560 012, India
[2]Division of Materials Science and Engineering, Department of Mechanical Engineering, The University of Akron, Akron, Ohio 44325 3903, USA

Reinforcement of magnesium alloys with ceramic particulates has engineered a new family of materials that are marketed under the trade name metal-matrix composites. Rapid strides in the processing of these materials during the last two decades have provided the necessary impetus for their emergence and use in structural and automotive-related components. In this article we report the results of a study aimed at understanding the role of particulate reinforcements on the tensile, compressive, impact deformation and overall fracture behaviour of magnesium alloy discontinuously-reinforced with silicon carbide particulates and saffil alumina short fibres. An increase in reinforcement content was observed to have a marginal influence on strength and detrimental influence on ductility compared to the un-reinforced counterpart. Microcracking in the metal matrix coupled with failure of the reinforcing phase (i.e. particulates or short fibres), both independently dispersed and in clusters, dominated the fracture sequence at the microscopic level. The deformation and final fracture behaviour of the composite materials are discussed in light of the concurrent and mutually interactive influences of microstructural effects, deformation characteristics of the composite constituents, nature of loading and local stress state.

DURING the last two decades, the need for new and improved materials has engendered considerable scientific and technological interest. The newer generation materials are used in a spectrum of performance-critical products in the industries of aerospace, automobile, power generation and even consumer-related products[1–4]. To meet this emerging need, innovations in materials processing enabled achieving an enhancement in stiffness, realization of high strength-to-weight ratio, an improvement in wear resistance, maintaining strength at elevated temperature, and enhanced resistance to corrosion when exposed to aggressive environments, while concurrently retaining other desirable properties based on end-applications[4,5].

In the early stages of materials development and emergence, the newer generation alloys offered acceptable specific stiffness (E/Y), high strength at the expense of ductility, and formability. Alternatively, pure metals and their alloy counterparts when reinforced with ceramic materials, offer notable improvement in existing properties[3,4,6,7]. The outcome of sustained research efforts resulted in the development and emergence of a family of reinforced materials referred to and marketed as composite materials[2–4]. The development of reinforced materials was based on choosing metal, intermetallic, ceramic or polymers as the matrix. Among the reinforced materials, metal-matrix composites (MMCs) have generated considerable scientific and technological interest, primarily because of the intrinsic advantages they offer with respect to: (a) processing, (b) fabrication using existing infrastructure, and (c) property development and/or enhancement[7]. Reinforced metal matrices of aluminum and its alloys have been the most widely used candidates for MMCs. Pure magnesium and its alloys also have their share of industrial applications, primarily because of: (a) their low weight, (b) good machinability, (c) excellent castability, (d) commendable weldability, (e) superior damping capacity, and (f) availability[8–11]. These properties have progressively strengthened the use of magnesium alloys in the aerospace and automobile industries[10,11]. Thus, both designers and manufacturers consider magnesium as a potentially viable and economically affordable candidate for selection as matrix for MMCs[6].

Soft, ductile and plastically deforming metal matrices discontinuously-reinforced (DR) with hard, brittle and elastically deforming reinforcements, i.e. DRMMCs, can be produced by stir-mixing, powder-metallurgy processes, thixo-casting, infiltration and squeeze-casting[2–5]. Recent research efforts have focused on use of the technique of squeeze-casting as a potentially feasible near net-shape casting process. This technique has grown in stature to account for the production of: (a) sizeable quantity of lightweight aluminum and zinc castings, and (b) comparatively lower quantity, but still substantial, of magnesium castings for use in automobiles and domestic machines[11,12]. Two unique advantages of the squeeze-casting technique are: (a) an ability to produce castings that are free from porosity, i.e. macroscopic and microscopic, and (b) the possibility of infiltrating molten metal/alloy into ceramic preforms to engineer composite materials[13].

Limited research efforts have been undertaken to produce and comprehensively characterize MMCs using mag-

*For correspondence. (e-mail: tsrivatsan@uakron.edu)

nesium as the matrix, i.e. MgMMCs. In particular, no comprehensive, industrially viable effort has been made to produce magnesium alloy-based composites using the squeeze-casting technique. Thus, there exists an interest driven by a need to develop magnesium-based composites using the squeeze-casting technique and to systematically characterize the microstructure and properties of the resultant composite. In the magnesium alloy family, magnesium–aluminum alloys are the most commonly chosen and extensively used candidates for structural applications[13–16]. However, exhaustive application of these alloys in performance-critical products is restricted primarily because they suffer from inadequate creep strength at temperatures above 120°C. This article concentrates on the alloy AM60 as the candidate for the metal matrix. The reinforcements used to strengthen the metal matrix are silicon carbide particulates (SiC_p) and saffil alumina (Al_2O_3) fibres. The influence of the nature (particulates vs fibres) and volume fraction of the reinforcing phase on mechanical response of the metal matrix is rationalized in light of competing and interactive influences of: (a) intrinsic composite microstructural effects, (b) properties of constituents of the composite, (c) deformation characteristics of the microstructure, and (d) macroscopic aspects governing fracture.

Materials

The study reported here involved reinforcing the magnesium–aluminum alloy with two different types of ceramics:

(a) SiC_p were introduced into the alloy melt through stirring, which resulted in the formation of a vortex. This was followed by squeeze-casting.
(b) In the case of alumina short-fibre reinforcements, the first step was the production of preforms using short Al_2O_3 fibres. The preforms produced were then infiltrated by the molten melt using an applied pressure during squeeze-casting.

SiC_p of average size 20 μm were procured from Carborundum Universal Ltd, India and the chopped alumina fibres from Saffil Ltd, United Kingdom. The magnesium alloy (AM60)-based composites produced were characterized for both microstructure and properties. The composites are denoted henceforth as AM60/SiC/xxp and AM60/Al_2O_3/xxf, where xx denotes volume fraction of the reinforcing phase and the terms p and f refer to the nature of the reinforcing phase: particulate (p) and fibres (f). Ageing studies were carried out on both the base alloy and the composite counterparts and the heat treatment sequence essential for achieving peak hardness was established. Also, (a) Young's modulus, (b) coefficient of thermal expansion (CTE), (c) tensile strength and compressive strength, and (d) impact behaviour were established. Fractography of the deformed and failed specimens was performed to rationalize the macroscopic fracture mode and the intrinsic mechanisms governing fracture at the microscopic level.

Materials processing

Particulate-reinforced metal matrices were produced with different volume fractions of SiC_p using the vortex method followed by squeeze-casting. Infiltration of molten magnesium into preforms of alumina, using the squeeze-casting technique, was chosen for the production of alumina fibre-reinforced composites. The nominal chemical composition of alloy AM60 is given in Table 1. The process sequence for producing the magnesium alloy (using pure metal ingot as the starting material) was optimized following a series of experimental trials and is summarized in Figure 1. Commercially pure magnesium was chosen as the starting metal. Ingots of pure magnesium were first cut into small pieces. The desired amount was then precision-weighed in a laboratory-scale balance to get 2 kg of the master alloy. In order to compensate for losses due to oxidation of the metal, the quantity taken was 20% more than the desired amount. The other key constituents in the alloy, i.e. aluminum, zinc, manganese and silicon were also precision-weighed so as to get the

Table 1. Nominal chemical composition of the magnesium alloy (in wt%)

Alloy Element	Mg	Al	Mn	Si	Cu	Zn	Ni
	92.27	5.5	0.3	0.5	0.35	0.22	0.04

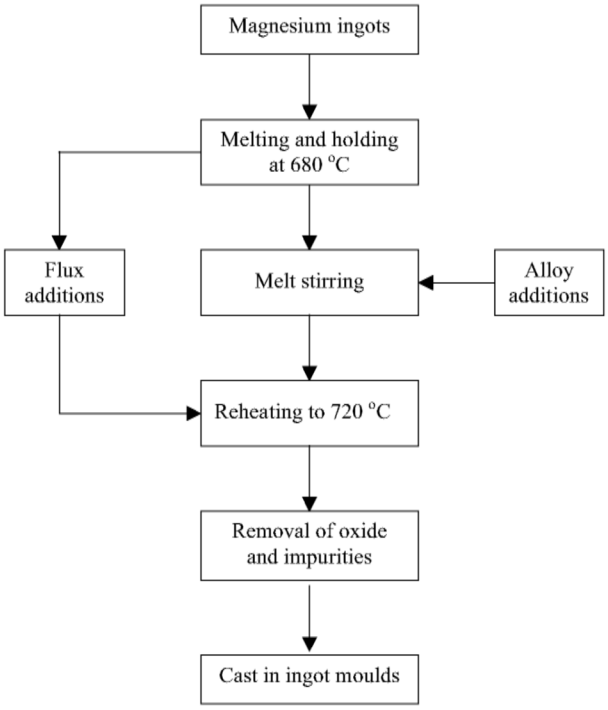

Figure 1. Processing sequence for magnesium alloy AM60.

recommended chemical composition. In order to account for possible losses during melting, the amount of manganese and zinc taken was 15% in excess of the desired value. Pieces of magnesium and aluminum were initially melted in an electric resistance furnace using a refractory crucible. About 1.0 wt% of flux was added to the crucible. The chemical composition of the flux used for the magnesium alloy is provided in Table 2. The furnace temperature was set at 680°C. Upon initiation of melting, the alloying elements were added and the molten metal was stirred using graphite rods. Upon completion of melting, the preheated flux was added and the resultant mixture stirred so that the flux can absorb all of the oxides and other impurities present in the molten metal. The molten metal was held at a temperature of 680°C for about 10 to 15 min so as to facilitate the sludge to settle down. The crucible was removed from the furnace and skimming eliminated dross collected at the top of the molten metal. The molten metal was poured into metallic ingot moulds that were pre-heated to 200°C. Both the die and punch used in the squeeze-casting machine were made of alloy steel. A coating of colloidal graphite was applied on the inside surfaces of both the die and punch prior to pouring, so as to facilitate easy removal of the casting following solidification. Steps were taken to ensure that the crucible was not completely emptied during pouring, so as to prevent the sludge that remained settled at the bottom of the crucible from entering the casting. The precise chemical composition of the base alloy ingot was assessed using vacuum emission spectrometer to verify that the composition conformed to specifications. The molten alloy melt was poured into a squeeze-casting die, followed by the application of r.a.m. pressure. The pressure was maintained for 45 s following which the solidified casting was ejected. The cylindrical cavity of the die used for producing squeeze-cast specimens measured 73 mm in diameter and 30 mm in height. The specifications for the squeeze-casting equipment are given in Table 3.

In an attempt to optimize mechanical properties, the particulate and fibre-reinforced magnesium alloy metal matrices were subjected to heat treatment to get the T5 temper. Test castings of alloy AM60 were examined for microstructure and properties following the T5 heat treatment: (i) direct quench from the casting temperature, and (ii) artificial ageing at 288°C for 2 h.

Table 2. Nominal chemical composition (in wt%) of the flux

Constituent	KCl	$MgCl_2$	MgO	CaF_2	$BaCl_2$
	37.5	42.0	7.5	8.5	4.5

Table 3. Specifications for squeeze-casting equipment

Press capacity	:	50 tons
Approach speed	:	100 mm/s
Return force	:	25 tons
Pressing speed	:	1 to 10 mm/s

Production of the SiC reinforced composite (AM60/SiC/xxp-T5)

The crucible containing melt of the alloy was placed in a large resistance furnace and held at the temperature of 700°C. A stirrer was introduced into the melt and stirring initiated. The speed of the stirrer was maintained at 600 ± 20 rpm. This rotational speed creates a vortex of adequate depth. The silicon carbide particulate reinforcing phase (pre-heated to 700°C) was gradually added to the vortex. Two different volume fractions, i.e. 10 and 15% were chosen and tried. Upon completion of addition of SiC_p to the molten melt, stirring of the mixture was continued for three additional minutes. The melt was then poured into squeeze-casting dies and immediately squeeze-cast at a constant pressure of 70 MPa.

Production of the fibre-reinforced composites

The squeeze-casting process (pressure infiltration) is also suitable for the production of MMCs, i.e. short fibres or whiskers reinforcing the metal matrix. The process consists of the following steps:

(a) Placing the preforms (made of fibres) in a die.
(b) Pouring molten metal over the preform.
(c) Infiltrating liquid metal into the porous space of the preform with the help of pressure or vacuum.

In this study, infiltration was achieved by pressurizing the liquid metal through hydraulically actuated piston of the squeeze-casting equipment. A pressure of 40 MPa was applied on the top surface of the melt within seconds of pouring. The applied pressure was maintained for 60 s causing the liquid metal to infiltrate into the fine pores in the preform; the resultant casting solidifies in a short duration. The solidified casting was ejected using a punch, as shown in Figure 2. Upon gradual cooling to room temperature (27°C), test specimens were precision-machined from the squeeze-cast ingot. On account of the greater hardness of the reinforced magnesium alloy MMCs polycrystalline diamond tools were essential for cutting and machining.

Experimental procedure

Microstructural characterization

Test specimens taken from both the un-reinforced (AM602) alloy and the composite counterparts (AM60/SiC/xxp-T5 and AM60/Al_2O_3/xxf-T5) were mechanically ground on progressively finer grades of silicon carbide-

impregnated energy paper using copious amount of water as lubricant. The ground specimens were then finish-polished using alumina (Al_2O_3) powder suspended in distilled water as lubricant, to near mirror-like surface finish. To reveal the intrinsic microstructural features, the mechanically ground and polished specimens were etched. The etchant is a solution mixture of acetic glycol and picral. The un-reinforced AM60 alloy was examined in an optical microscope (Leitz: Metallovert D), while the reinforced metal matrix (AM60/SiC/xxp-T5) was examined in a scanning electron microscope (JEOL JSM-840A) to facilitate high magnification observations of the reinforcing phase (SiC_p) and its distribution in the metal matrix.

Mechanical testing

The Young's modulus was independently assessed using the 'elastosonic' equipment, which is based on the principle of ultrasonic non-destructive testing.

The coefficient of thermal expansion (CTE) of the test specimen was assessed using a thermal analyser, by the contact method, over a range of 70–400°C. The specimens, kept in a quartz container, were heated to a predetermined temperature. Expansion of a chosen sample was assessed in terms of voltage and appropriately converted to a change in length. The thermal analyser was attached to a computer-based data acquisition system (DAS). A plot depicting the variation of temperature (°C) with elongation was obtained. From this plot, CTE of the material was calculated.

The hardness of both the un-reinforced alloy (AM60-T5) and the composites (AM60/SiC/xxp-T5 and AM60/Al_2O_3/xxf-T5), subsequent to T5 heat treatment, was determined using the Brinell Hardness Test machine. The indenter used was a 10 mm steel ball and the applied load was 500 kgf. An optimum ageing sequence was established for both the un-reinforced alloy and the reinforced counterpart. It was essentially observed that the AM60/SiC/xxp-T5 and AM60/Al_2O_3/xxf-T5 composites took considerably less time to reach peak hardness compared to the un-reinforced counterpart (AM60-T5).

Tensile tests were carried out on a 100 KN fully automated, computer-controlled, servo-hydraulic universal test machine (Model: INSTRON). The dimension of the test specimen conformed to specifications stipulated in ASTM Standard E-8 (ref. 17). The test specimens were deformed to failure at room temperature (27°C), laboratory-air environment (relative humidity 55%) at a constant strain rate of 0.01/s.

Uniaxial compression tests (to determine the ultimate compressive strength) were carried out at both room and elevated temperatures on a 100 KN capacity fully automated, computer-controlled, servo-hydraulic mechanical test machine (Model: DARTEC). In this test machine, the strain rate was maintained as low as 0.01/s. The test machine has provisions for testing at elevated temperatures up to 1200°C. The compression test samples were cylindrical in shape having a diameter of 10 mm and a length of 15 mm. The compression tests were performed at 27 and 350°C on both the un-reinforced alloy (AM60-T5) and the composites (AM60/SiC/xxp-T5 and AM60/ Al_2O_3/xxf-T5). The furnace was maintained at a pre-determined temperature and the specimens were soaked for a full 15 min prior to the initiation of testing.

Impact (Charpy V-notch) tests were carried out on both the un-reinforced alloy (AM60) and the composites (AM60/SiC/xxp-T5 and AM60/Al_2O_3/xxf-T5) using a constant striking velocity, so as to assess the total energy absorbed prior to catastrophic failure and the resultant value of K_{IC}. The tests were carried out on a fully instrumented Charpy impact test machine having a DAS. The test data were processed using DYNATUP software to get the total energy absorbed and the value of K_{IC}. The tests were carried out at room temperature (27°C), laboratory-air environment (relative humidity of 55%) on standard CVN test specimens, which conformed to specifications outlined in the ASTM Standards[18].

Failure-damage analysis

The fracture surfaces of the deformed and failed tensile, compression and impact test specimens were examined in

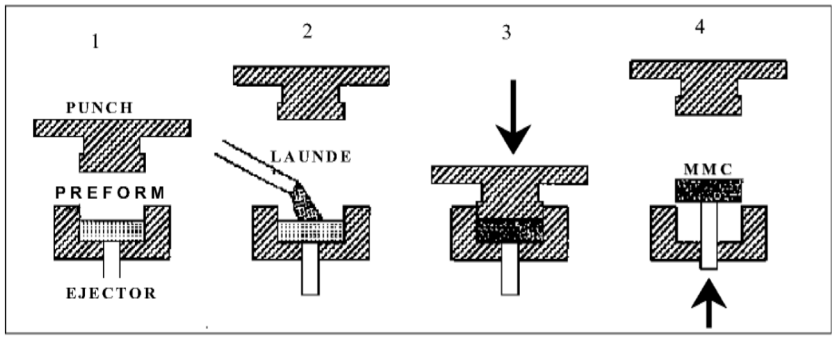

Figure 2. Production process for squeeze-cast composite using fibre preforms.

a scanning electron microscope (Model: JEOL-JSM-84A) to: (a) determine the macroscopic fracture mode, and (b) characterize the fine-scale topography and microscopic mechanisms governing fracture. The overall distinction between the macroscopic mode and microscopic fracture mechanisms is based on the magnification level at which the observations are made.

Results and discussion

Microstructure of alloy AM60

Optical microstructure of the gravity-die-cast AM60 alloy is shown in Figure 3 *a* and reveals coarse grains of varying size. However, optical microscopy examination of the squeeze-cast counterpart, shown in Figure 3 *b*, reveals finer grain morphology. The observed drastic refinement in grain size of the squeeze-cast alloy compared to the die-cast counterpart is attributed to higher solidification rate of the molten metal resulting from enhanced rate of heat extraction. The key phases present in the microstructure, at different temperatures, during solidification of alloy AM60 are summarized in Table 4. Essentially, the microstructure of alloy AM60 consists of: (a) solid solution phase (magnesium), (b) eutectic magnesium (super-saturated solid solution) and (c) intermetallic $Mg_{17}Al_{12}$. The microstructure of the alloy following the T5 heat-treatment sequence is shown in Figure 4.

Figure 5 is an optical micrograph showing a near uniform distribution of the reinforcing SiC_p in the magnesium alloy (AM60) metal matrix. High magnification observations revealed the absence of debonding between the reinforcing SiC_p and the magnesium alloy metal matrix. A near uniform distribution of saffil alumina fibres was also observed for the short fibre-reinforced magnesium alloy metal matrix. This clearly suggests that the method of preform preparation used in this study is effective, resulting in a near uniform distribution of the reinforcing phase (fibres) in the metal matrix.

Ageing kinetics of alloy AM60

Ageing response data obtained on alloy AM60 assist in heat treatment optimization. The response of the alloy to ageing is shown in Figure 6. Owing to the faster rate of solidification encountered during squeeze-casting, the resultant specimens exhibit a much finer grain size compared to the die-cast counterpart. Consequently, the squeeze-cast product (specimen) has a much higher value of peak hardness than its die-cast counterpart. Table 5 summarizes peak hardness value and the corresponding time to reach peak hardness for the reinforced magnesium alloy metal matrix.

When the alloy AM60 is reinforced with SiC_p, the ageing response is accelerated with a concurrent increase in peak hardness compared to the un-reinforced alloy. The observed increase in hardness is ascribed to the concurrent and mutually interactive influences of: (a) the presence of the reinforcing SiC_p phase and (b) a finer grain size of the composite microstructure. Similar findings have been reported by Guden and Hall[19]. The accelerated ageing curve of alloy AM60 reinforced with SiC

Table 4. Phases present during solidification of alloy AM60

Process	Temperature (°C)
Solidification of solid solution (magnesium) from molten liquids	615
Growth of solid solution (Mg) from liquid. Liquid gets enriched in aluminum	615–437
Mg (solid solution) growth ends. Liquid reaches eutectic temperature	> 437
Liquid solidifies as two phases: eutectic and $Mg_{17}Al_{12}$	437
Slow diffusion rates of aluminum in magnesium allows the eutectic to remain present as a super-saturated solid solution	437 to room temperature

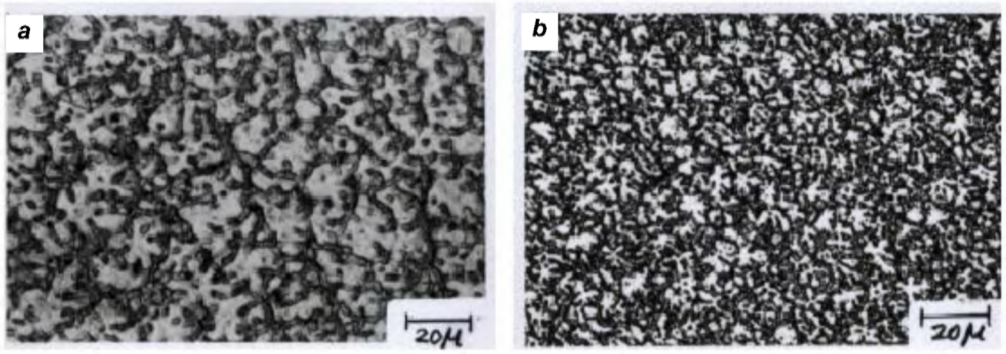

Figure 3. Optical micrographs showing microstructure of alloy AM60: (***a***) Gravity die cast and (***b***) squeeze-cast.

and saffil alumina short fibres is shown in Figure 7. One may conclude that:

(a) Peak hardness of the reinforced magnesium alloy is significantly higher than the peak hardness of the unreinforced counterpart. The enhanced hardness of the composite material is ascribed to the conjoint and mutually interactive influences of: (i) an increased dislocation density in the microstructure and (ii) the presence of hard, brittle and essentially elastically deforming reinforcing phase in the soft, ductile and predominantly plastically deforming metal matrix[3,4].

(b) Presence of SiC_p and saffil alumina short fibre reinforcements decreases the time needed to reach peak hardness in comparison with the un-reinforced counterpart.

(c) The observed difference in hardness values ($H = H_{max} - H_o$) due to ageing for both the composite material and the un-reinforced metal matrix is almost the same. This indicates that while the amount of strengthening phases present in the composite microstructure is significantly more than in the un-reinforced counterpart, other factors such as size and distribution of the strengthening phases, also play an important role and these may have opposite effects.

(d) The gradual decrease in hardness of the materials upon reaching a peak value, is faster for the reinforced magnesium alloy metal matrix than for the un-reinforced counterpart. The presence of a high dislocation density both at and near the reinforcement-matrix interfaces coupled with the precipitation and growth of precipitates at the interfaces in the composite microstructure is faster, while overall dissolution rate of the precipitate is slower. The increased growth rate of the strengthening precipitates, both at and near interfaces, is conducive to enhanced dissolution rate of the precipitates located well within the grain interior. This is responsible for the observed decrease in hardness of the material.

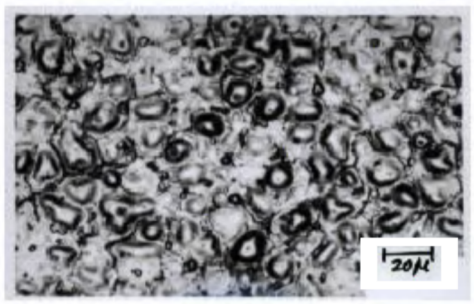

Figure 4. Optical micrograph showing microstructure of squeeze-cast magnesium alloy AM60 following T5 heat-treatment sequence.

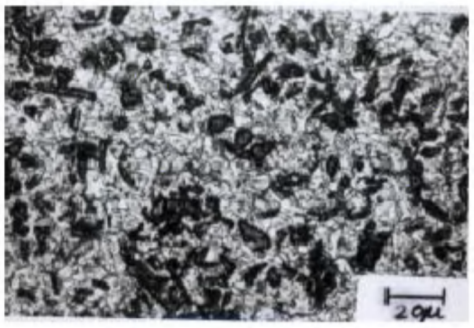

Figure 5. Optical micrograph of the alloy metal matrix reinforced with SiC_p showing near uniform distribution of the reinforcing phase in the metal matrix.

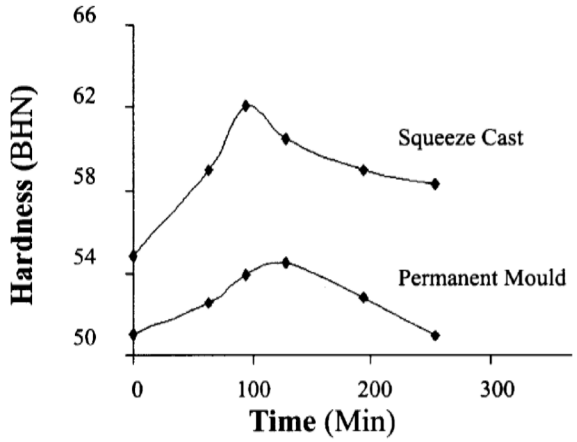

Figure 6. Influence of primary processing (permanent mould cast vs squeeze-cast) on ageing response of alloy AM60.

The key mechanism responsible for accelerated ageing of the reinforced magnesium alloy metal matrix is increased dislocation density, arising from differences in the CTE of the composite constituents, i.e. the soft metal matrix and the hard reinforcement phase (particulates and short fibres) in the vicinity of the reinforcing phase[3,20]. The higher dislocation density facilitates the diffusion of solute atoms to reinforcement-matrix interfaces[21], while also serving as potential nucleation sites arising from a decrease in incubation time for nucleation[22]. Preferential precipitation on dislocations is responsible for the observed exacerbation in ageing response of the reinforced magnesium alloy metal matrix[23].

Modulus of elasticity

Elastic modulus is a direct measure of stiffness. The stiffness of the reinforced metal matrix was determined by

Table 5. Peak hardness of alloy AM60 and composites

Material	Peak hardness (BHN)	Time to reach peak hardness (s)
AM60 (die-cast)	55.15	120
AM60 (squeeze-cast)	63.56	90
AM60/SiC/10p-T5	74.44	30
AM60/SiC/15p-T5	79.54	20
AM60/$A1_2O_3$/25f-T5	145.12	20
AM60/$A1_2O_3$/30f-T5	149.34	10

the elastosonic method and also calculated using the simple rule-of-mixtures (ROM) theory:

$$E_{\text{composite}} = E_M V_M + E_f V_f, \quad (1)$$

where E_M is Young's modulus of the metal matrix, E_f is the Young's modulus of the reinforcing phase, V_M is volume fraction of the metal matrix, and V_f is volume fraction of the reinforcing phase.

From the relevant values and using the eq. (1), the specific stiffness (E/Y) was calculated for each material (where Y is the density of the material). These values are summarized in Table 6. The ROM gives the upper-bound estimate of the elastic modulus, since it is modelled based on an assumption of iso-strain condition. The ROM (iso-strain condition) is considered to be accurate for predicting the longitudinal modulus of both the continuous fibre-reinforced metal matrices and aligned short fibre-reinforced metal matrices. However, it fails to provide an accurate estimate for stiffness of the metal matrix reinforced with randomly oriented short fibres.

As the volume fraction of the reinforcement phase (both particulates and fibres) in the metal matrix increases, the amount of reinforcements that are well bonded to the metal matrix increases. Thus, stress transferred from the ductile magnesium alloy metal matrix to the hard and brittle reinforcing phase is higher as volume fraction increases due to a local increase in interfacial area. With an increase in stress, interface debonding is favoured to occur at the heavily loaded reinforcing phase. This was evident on high magnification observation of the tensile fracture surfaces. A gradual increase in applied load initiates fine microscopic cracks at:

(i) The loosely bonded short fibres and SiC_p reinforcements independently dispersed through the metal matrix.
(ii) Locations of reinforcement agglomeration.

Numerous fine microscopic cracks were distinctly evident in the metal matrix at locations of reinforcement agglomeration. High magnification observations revealed shallow dimples scattered through the metal matrix.

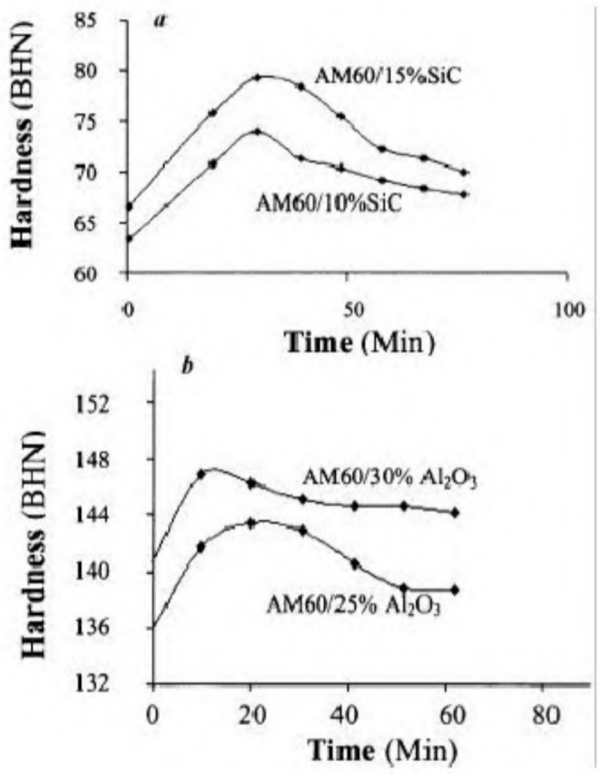

Figure 7. *a*, Influence of volume fraction of particulate reinforcement on ageing response of magnesium alloy AM60. *b*, Influence of saffil short fibre reinforcement on ageing.

Coefficient of thermal expansion

The simplest model for predicting the CTE for the reinforced magnesium alloy metal matrix is the ROM approximation.

$$\Delta_{\text{composite}} = \Delta_M V_M + \Delta_f V_f, \quad (2)$$

where $\Delta_{\text{composite}}$ is CTE of the composite microstructure, Δ_M is coefficient of thermal expansion of the matrix, Δ_r is CTE of the reinforcing phase, and V represents volume fraction of the phase.

Equation (2) was used to estimate CTE of the particulate-reinforced metal matrix. However, for the short fibre-reinforced metal matrix, predictions using this model are dependent on l/d ratio, and fibre misorientation. The model proposed by Schapery[19] is simple and predicts

Table 6. Elastic modulus (Young's Modulus) of alloy AM60 and composite constituents

Material	Young's modulus		Density [Y] g/cm^3	Specific stiffness [E/Y]
	From experiment	From ROM		
AM60	45	–	1.8	–
AM60/SiC/10p-T5	49	84	2.01	41.5
AM60/SiC/15p-T5	68	103	2.07	49.6
AM60/Al_2O_3/25f-T5	74	109	2.23	48.8
AM60/Al_2O_3/30f-T5	87	121.5	2.27	54

reproducible values for CTE for the short fibre-reinforced metal matrices:

$$\Delta = \{E_1 \Delta_1 f + E_M \Delta_M (1-f)\}/\{E_1 f + E_M (1-f)\}, \quad (3)$$

where Δ_1 is CTE of the reinforcing fibre in the axial direction, Δ_M is CTE of the metal matrix, E_1 is Young's modulus of the fibre, E_M is Young's modulus of the matrix and f denotes volume fraction of the phase. The experimentally measured and calculated values of CTE are summarized in Table 7. For a given reinforcement selection and volume fraction, the value of CTE of the composite microstructures (AM60/SiC/xxp-T5 and AM60/Al_2O_3/xxf-T5) is lower than the un-reinforced counterpart (AM60-T5). Assuming adequate interfacial bonding between the soft metal matrix and the hard reinforcing phase, and absence of debonding during thermal cycling the thermal expansion of the composite will be closer to the calculated value.

Tensile response

Composite AM60/SiC/xxp–T5 – Tensile properties: Influence of volume fraction of reinforcement on tensile yield strength and ultimate strength of alloy AM60 and the composite counterparts (AM60/SiC/xxp and AM60/Al_2O_3/xxf) are shown as bar graphs in Figure 8. The ultimate tensile strength decreases, while 0.2% offset yield strength increases on reinforcing alloy AM60 with different volume fractions of the particulate phase (SiC). The influence of volume fraction of the reinforcing ceramic phase on tensile properties is summarized in Table 8. Yield strength of the SiC_p reinforced magnesium alloy metal matrix is marginally higher than that of the un-reinforced counterpart (AM60-T5). However, tensile strength and per cent elongation of the composite material are noticeably lower than those of the un-reinforced counterpart, for both volume fractions of the particulate reinforcement phase in the magnesium alloy metal matrix.

Table 7. Coefficient of thermal expansion of alloy AM60 and composite counterparts

Material	Coefficient of thermal expansion ($\times 10^{-6}$ C)	
	Experimental	Calculated
AM60 (die-cast)	25.6	–
AM60 (squeeze-cast)	2.4	–
AM60/SiC/10p-T5	23.01	23.31
AM60/SiC/15p-T5	19.9	22.44
AM60/Al_2O_3/25f-T5	10.72	11.20
AM60/ Al_2O_3/30f-T5	9.97	10.19

The observed drop in tensile strength and ductility (i.e. elongation) is attributed to the non-uniform distribution of the reinforcing SiC_p in the magnesium alloy metal matrix exacerbated by the tendency of SiC_p, both independently dispersed in the metal matrix and also at locations of particulate clustering or agglomeration, to be susceptible to premature cracking. The rate of strain hardening is higher for the composite microstructures and the concomitant increase in yield strength.

Tensile fracture: Examination of the tensile fracture surfaces in a scanning electron microscope revealed bimodal failure, i.e. a combination of transgranular and intergranular regions. In locations where the matrix (magnesium alloy) phase was dominant, the fracture was predominantly ductile. However, regions rich in reinforcing SiC_p revealed features reminiscent of locally brittle failure (Figure 9 *a*). Overall, the tensile fracture surface revealed a combination of shallow dimples (Figure 9 *b*) of varying sizes and failure of the reinforcing SiC_p through cracking (Figure 9 *c*), and decohesion at interfaces with the metal matrix (Figure 9 *d*), features reminiscent of locally ductile and brittle failure mechanisms. The fine microscopic cracks observed on surfaces of the reinforcing SiC_p could also have been caused by the thermal shock induced either during solidification or quenching (Figure 9 *c*). Cracking of the reinforcing SiC_p suggests the existence of strong bonding at the interfaces with the metal matrix. Quenching during heat treatment favours a large dislocation density at matrix-reinforcement interfaces due to intrinsic mismatch in CTE between constituents of the composite. The dislocations cause a local increase in stress and are conducive for enhancing the likelihood of particulate fracture during deformation[25].

Agglomeration or clustering of the reinforcing SiC_p was evident on tensile fracture surfaces. Overall, at locations of particulate agglomeration, there was no distinct evidence of the metal matrix (Figure 10 *a*). Fine intergranular cracks were also observed in the failed tensile specimens of the composite. It is probable that the fine microscopic cracks are formed as a result of hot tearing, which occurs during solidification.

Table 8. Uniaxial tensile properties of alloy AM60 and composite constituents

Material	Ultimate tensile strength (MPa)	Yield strength (MPa)	Elongation (%)
AM60	24	122	9.6
AM60/SiC/10p-T5	219	128	4.2
AM60/SiC/15p-T5	211	132	2.3
AM60/Al_2O_3/25f-T5	240	140	1.7
AM60/Al_2O_3/30f-T5	247	144	1.3

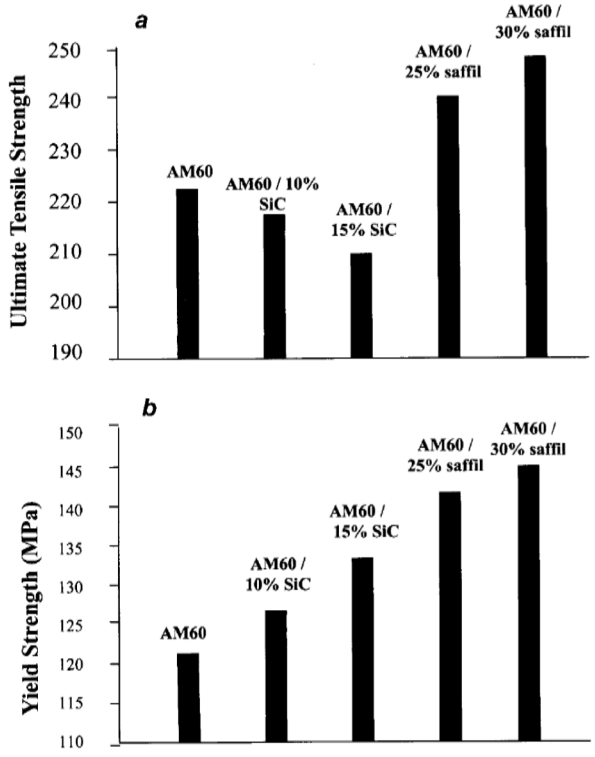

Figure 8. Bar graph showing influence of (*a*) volume fraction of reinforcement on tensile strength and (*b*) reinforcement on yield strength of magnesium alloy AM60.

There was a thin layer of magnesium at and away from the matrix-reinforcement interfaces (identified by EDAX analysis), which covered the surfaces of the particle (Figure 10 *b*). A transition in fracture mechanism from bimodal, i.e. combination of decohesion at the matrix-reinforcement particle interfaces and particulate failure by cracking, to predominant failure of the particulate by cracking was observed with an increase in volume fraction of the reinforcement in the magnesium alloy metal matrix.

AM60/Al_2O_3/xxf-T5 – Tensile properties: The yield strength and tensile strength of the fibre-reinforced metal matrix are marginally higher than those of the un-reinforced counterpart. With an increase in volume fraction of the fibre-reinforcing phase in the magnesium alloy metal matrix, both yield strength and ultimate tensile strength of the metal matrix increase, while per cent elongation, a measure of ductility, shows a marginal decrease. This may be due to an increase in effective yield strength of the composite microstructure due to constraints in deformation induced by the reinforcing fibres. The ductility, quantified by per cent elongation, of the un-reinforced alloy is concurrently reduced. At ambient temperature, the reinforced magnesium alloy metal matrices fail at around 1% strain, while failure of the un-reinforced (AM60) counterpart is around 9.6%. The decrease in failure strain is attributed to two competing mechanisms: (i) Presence of thermal residual stresses in the reinforced

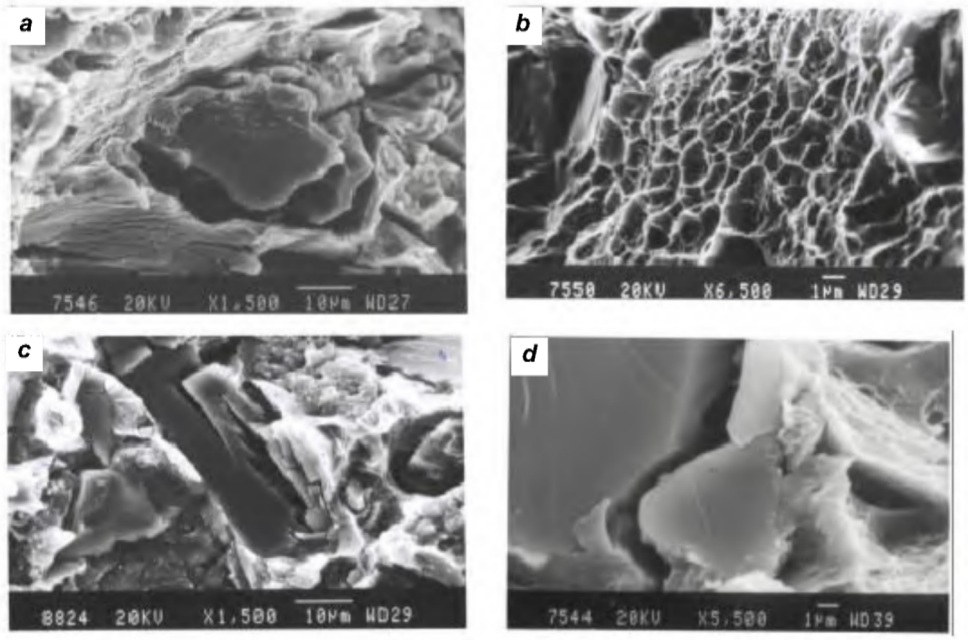

Figure 9. Scanning electron micrographs of tensile fracture surface of AM60/SiC/xxp composite showing: ***a***, Ductile failure in the matrix and brittle failure at the reinforcing phase (SiC); ***b***, Fine shallow dimples in regions between the reinforcing SiC_p. ***c***, Failure of the reinforcing SiC_p by cracking; ***d***, Debonding at the interface between the metal matrix and the reinforcing SiC_p.

metal matrix and (ii) load transfer from the plastically deforming metal matrix to the elastically deforming fibre reinforcements.

The first mechanism arises as a result of differences in CTE of the composite constituents, i.e. fibre and metal matrix. The second mechanism suggests that even when the short alumina fibre fails, the matrix transfers the load to other fibres as also to the same fibre at other locations/positions[24–26].

Tensile fracture: Observation of tensile fracture surfaces reveals that the failure of the composite is mixed mode, comprising ductile and brittle regions (Figure 11 *a*). The matrix revealed a combination of dimples (Figure 11 *a*) and isolated pockets of cleavage. High magnification observations of the tensile fracture surfaces revealed that the final fracture resulted from the fine microscopic cracks not passing through the fibres but around the fibres (Figure 11 *b*). Debonding between the short fibre reinforcement and the magnesium alloy metal matrix was distinctly evident (Figure 11 *c*). There was evidence of micro-plastic deformation, i.e. dimples, in the matrix between the reinforcing fibres at locations where the fibre ends were exposed on the surface. It appears that the alloy matrix sheared away from the fibre ends leaving behind metal adherences (Figure 11 *d*).

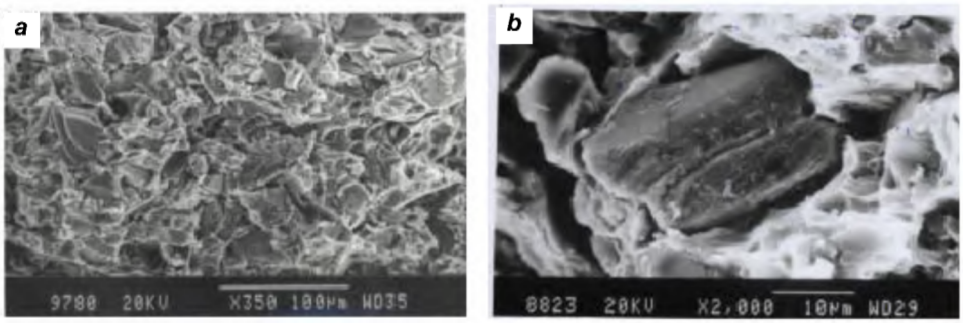

Figure 10. ***a***, Scanning electron micrograph of tensile fracture surface of composite AM60/SiC/xxp-T5, showing agglomeration and/or clustering of the reinforcing particulates. ***b***, Scanning electron micrograph of the AM60/SiC composite revealing thin layer of magnesium, identified by EDAX, between the reinforcing SiC particulate and the soft magnesium alloy metal matrix.

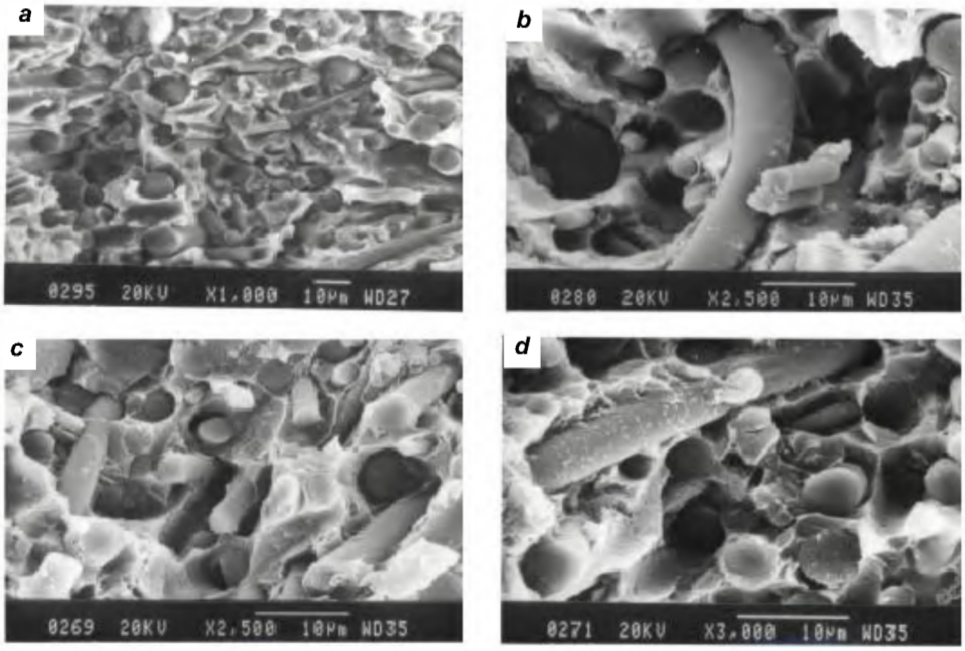

Figure 11. Scanning electron micrograph of the AM60/Al_2O_3/xxf-T5 composite showing: ***a***, Mixed mode failure comprising transgranular and inter-granular regions; ***b***, Failure of the reinforcing short fibres by buckling; ***c***, Debonding between reinforcing short fibre and magnesium alloy metal matrix; ***d***, Localized shearing in the metal matrix away from the fibre ends.

Compressive strength

The compression strength of the un-reinforced alloy AM60 increases with addition of ceramic reinforcement to the magnesium alloy metal matrix. Figure 12 is a bar graph depicting the compressive strength of alloy AM60 and composite counterparts when deformed in compression at 200°C. At this elevated temperature, the compression strength of the reinforced metal matrix is noticeably higher than the un-reinforced counterpart. There is an observed increase in compression strength of the metal matrix reinforced with 15 vol.% of SiC_p (about 100 MPa) over the un-reinforced counterpart. The noticeable increase in compression strength is attributed to partial closure of the fine microscopic cracks during compression loading. Compressive strength of the short fibre-reinforced metal

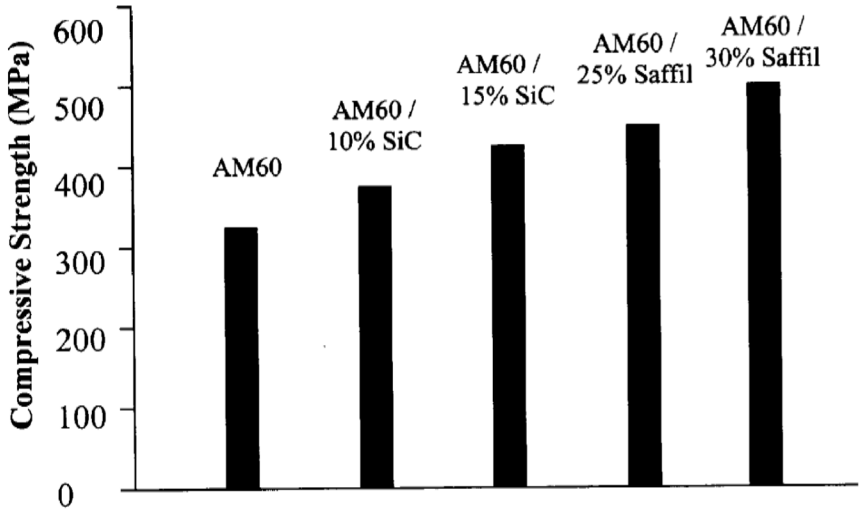

Figure 12. Bar graph showing the influence of reinforcement type and volume fraction on compressive strength of magnesium alloy AM60 for samples deformed in compression at 200°C.

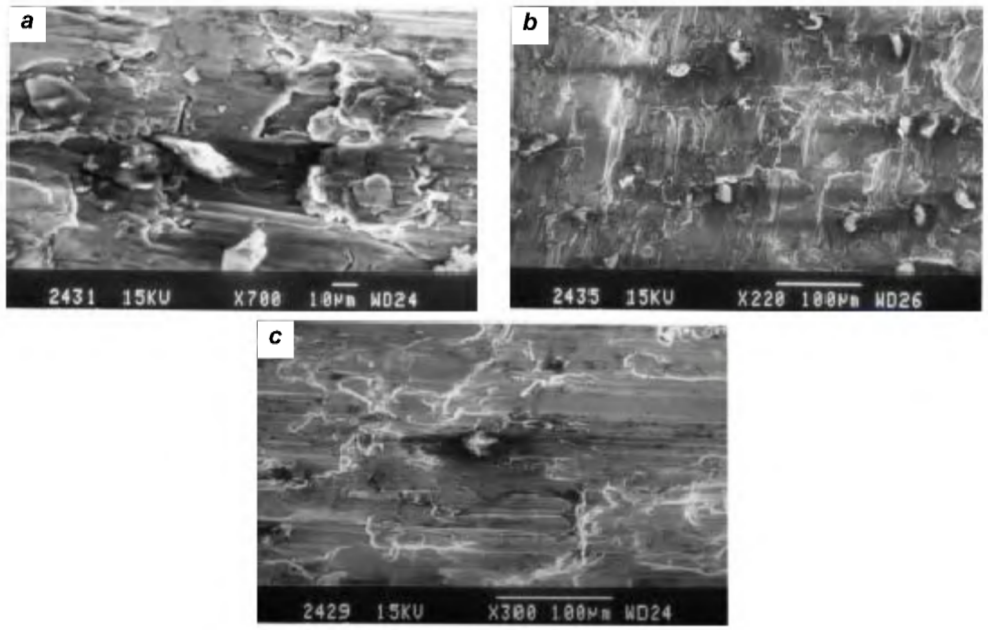

Figure 13. Scanning electron micrograph of fracture surface features of the sample deformed in compression showing: ***a***, Different flow patterns in the metal matrix due to the presence of reinforcing particulates; ***b***, Reinforcing SiC_p oriented along the shearing direction of the matrix; ***c***, Debonding at matrix–particulate interfaces.

matrix (AM60) is significantly higher than that of the unreinforced counterpart. The increase in strength is as high as 200 MPa.

Scanning electron microscope observations of the deformed sample revealed different flow patters within the metal matrix and at locations of the hard, brittle and elastically deforming SiC_p. Some of the reinforcing SiC_p were oriented along the direct load axis (Figure 13 *b*). Micro-plastic deformation was evident in the matrix between reinforcing particulates. The metal matrix both at and near the corners of the reinforcing SiC_p revealed greater deformation compared to material located farther away from the reinforcing particulates (Figure 13 *c*). Highly localized debonding was evident at the interfaces between the alloy matrix and the reinforcing particulates (Figure 13 *d*).

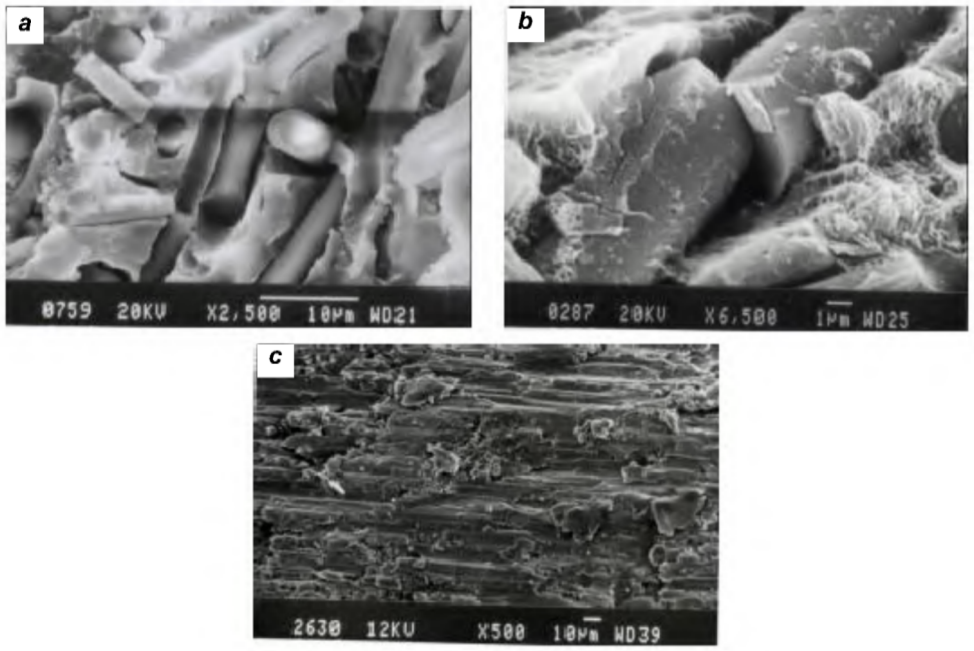

Figure 14. Scanning electron micrograph of short fibre-reinforced magnesium alloy deformed in compression showing: ***a***, Failure of reinforcing fibre by buckling; ***b***, Shearing of fibre in matrix-rich regions; ***c***, Evidence of localized micro-plastic deformation in matrix-rich regions.

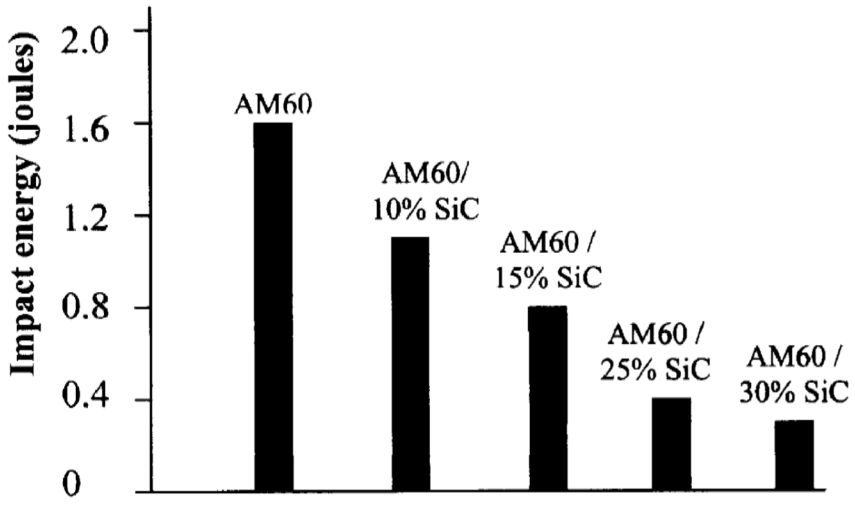

Figure 15. Influence of ceramic reinforcement (particulates or fibres) on impact energy of magnesium alloy AM60.

Table 9. Plane strain fracture toughness (K_{IC}) values of alloy AM60 and composite counterparts

Material	Plane-strain fracture toughness MPa $(m)^{0.5}$
AM60	16.45–17.11
AM60/SiC/xxp-T5	13.22–15.67
AM60/Al_2O_3/xxf-T5	9.12–9.88

Exhaustive scanning electron microscopy observations of the short fibre-reinforced samples revealed the following:

(a) Regions smeared and devoid of distinctly clear features due to rubbing of the mating fracture surfaces during shear failure (Figure 14 *a*).
(b) Pockets of shallow dimples, reminiscent of locally ductile failure, and debonding at the fibre–matrix interfaces, reminiscent of locally brittle failure.

The short fibres that were positioned at an angle to the far-field stress axis, i.e. load axis, fractured either by buckling or shearing (Figure 14 *b*). Buckling was more evident in those fibres that were closely placed. However, shearing was dominant in the matrix-rich regions and at locations where the short fibres were inclined at an angle to the load axis (Figure 14 *b*). The short fibres located/positioned normal to the far field stress axis fractured easily. The closely spaced fibres fractured in the normal plane due to an absence of matrix ductility and crack-tip blunting. The deformed fibres were fragmented, providing evidence for the effectiveness of load transfer and overall homogeneity of deformation in the compression tests[26]. Void formation, such as that observed during tensile loading of the short fibre-reinforced composites, was not apparently evident in the microstructure, primarily because it is suppressed by compressive hydrostatic pressure (Figure 14 *c*).

This is the most appealing rational for enhanced tendency for localized micro-plastic deformation of the composite samples when subjected to compression loading[25].

Impact behaviour

The impact behaviour of the composite with the un-reinforced counterpart is compared in Figure 15. The impact energy value of the composites is marginally lower than that of the un-reinforced alloy (AM60-T5). As volume fraction of the reinforcing phase (particulates or fibres) in the magnesium alloy metal matrix increases, the impact energy of the composite microstructure decreases compared to the un-reinforced magnesium alloy metal matrix. The K_{IC} values of the monolithic alloy and the composite counterparts are given in Table 9. Scanning electron microscope observations of the fracture surfaces of deformed samples revealed bimodal failure, with regions rich in transgranular and intergranular fracture features. Higher magnification revealed a population of fine microscopic voids scattered through the fracture surface. Also evident were fine microscopic cracks, reminiscent of locally brittle failure mechanisms[26].

Conclusion

(1) Optical microstructure revealed a near uniform distribution of the reinforcing phase, be it particulates of silicon carbide or short fibres of alumina, in the metal matrix. This suggests that the processing methods used for both particulate-reinforced and fibre-reinforced MMCs are effective and appropriate.
(2) The grain size of the squeeze-cast alloy (AM60) was much finer than the die-cast counterpart. The influence of squeeze-casting on grain structure development is attributed to the high initial rate of heat extraction.
(3) Ageing response of the ceramic-reinforced magnesium alloy, quantified in terms of hardness, is higher compared to the un-reinforced matrix alloy. This is ascribed to: (a) constraints in mechanical deformation of the alloy microstructure by the reinforcing phase and (b) the presence of increased dislocation density arising as a result of large difference in coefficient of thermal expansion between constituents of the composite.
(4) Coefficient of thermal expansion of the AM60/SiC/xxp and AM60/Al_2O_3/xxf composites are lower than the un- reinforced alloy. This is partially because the reinforcing phase (SiC and Al_2O_3) has lower CTE than magnesium.
(5) The Young's modulus of the reinforced metal matrix is marginally higher than that of the un-reinforced alloy. The modulus increases with an increase in volume fraction of the reinforcing phase (particulates or fibres) in the metal matrix.
(6) The yield strength and ultimate tensile strength of AM60/SiC/xxp-T5 MMCs is higher than the un-reinforced counterpart. However, ductility, i.e. per cent elongation is marginally lower than that of the un-reinforced alloy for all volume fractions of reinforcement in the magnesium alloy metal matrix. The compressive strength of the reinforced metal matrix is higher than that of the un-reinforced counterpart.
(7) The observed increase in compressive strength of the metal matrix reinforced with SiC_p is as high as 15%. The marginal increase in compressive strength is attributed to the influence of reinforcement in altering deformation characteristics of the composite microstructure.
(8) The impact energy values of the reinforced metal matrix are lower than those of the un-reinforced counterpart. The decrease in toughness is ascribed to the presence of intrinsic microstructural defects in the composite microstructure.

1. Nair, S. V., Tien, J. K. and Bates, R. C., SiC-reinforced aluminium metal matrix composites. *Int. Met. Rev.*, 1985, **30**, 275–290.
2. Lewandowski, J. J., Fracture and fatigue of particulate composites. *Metal Matrix Composites* (ed. Clyne, T. W.), Elsevier Publishers, New York, 2000, vol. 3, pp. 151–187.

3. Taya, M. and Arsenault, R. J. (eds), *Metal Matrix Composites: Thermo-mechanical Behavior*, Pergamon Press, New York, 1989.
4. Srivatsan, T. S. and Sudarshan, T. S., Mathematical modeling of rapid solidification. In *Rapid Solidification Technology: An Engineer's Guide*, Technomic Publishing Company, Lancaster, USA, 1993, pp. 3–70.
5. Srivatsan, T. S., Sudarshan, T. S. and Lavernia, E. J., Processing of discontinuously-reinforced metal matrix composites by rapid solidification. *Prog. Mater. Sci.*, 1995, **39**, 317–409.
6. Christman, T. and Suresh, S., Microstructural development in an aluminum alloy–SiC whisker composite. *Acta Metall.*, 1988, **36**, 1699–1704.
7. Clyne, T. W. and Withers, P. J., *An Introduction to Metal Matrix Composites*, Cambridge University Press, Cambridge, 1995, pp. 1–525.
8. Spare, N. C., Modern strategy for magnesium in automobiles: In Design Prospects and Material Aspects and Magnesium Technology, Proceedings of London Conference, 1986, pp. 101–106.
9. Unsworth, W., New ZCM magnesium alloys. SAE Technical Paper No. 880512, 1988, pp. 2.32–2.37.
10. *Magnesium Die Casting Handbook*, NADACA, 1998.
11. Schumann, S. and Friedrich, F., The Use of Magnesium in Cars: Today and in Future. *Magnesium*, 1998, 3–13.
12. Baker, C. F. and Mercer, W. E., Innovative shot delivery system for magnesium. SAE Technical Paper Series No. 920068, 1992, 1–6.
13. Thomas, R. J. and Darryl, A., Magnesium castings for auto applications. *Adv. Mat. Proc.*, 1994, **145**, 28–32.
14. Froes, F. H., Rapid solidification of lightweight metal alloys A. *Mater. Sci. Eng.* 1989, **117**, 19–32.
15. Lavernia, E. J., Baram, J. and Gutierrez, E., Precipitation and excess solid solubility in Mg–Al–Zr and Mg–Zn–Zr processed by spray atomization and deposition. *Mater. Sci. Eng. A*, 1991, **132**, 119–133.
16. Polmear, I. J., Magnesium alloys and applications. *Mater. Sci. Technol.*, 1994, **10**, 1–16.
17. ASTM Standard E-8, 'Standard test method for tension testing of metallic materials'. American Society for Testing and Materials, Race Street, Philadelphia, PA, USA, 1993.
18. ASTM Standard E23: 'Standard test method for impact test method for impact testing of metallic materials', American Society for Testing and Materials, Race Street, Philadelphia, PA, USA, 1993.
19. Schapery, R. A., A theory of mechanical behavior of elastic media with growing damage and other changes in structure. *J. Mech. Phys. Solids*, 990, **38**, 215–253.
20. Guden, M. and Hall, I. W., Dynamic properties of metal matrix composites: a comparative study. *Mater. Sci. Eng. A*, 1998, **242**, 141–153.
21. Blair, E. C., The effect of strain rate and temperature on the deformation of die cast AM60b. SAE technical paper no. 950425, 1995, 343.
22. Terje, K. A. and Hakon, W., Magnesium die casting properties. *Automotive Eng.*, 1995, **103**, 87–92.
23. Terje, K. A. and Riopelle, L. A., Evaluation of the mechanical properties critical to the design of interior magnesium components. SAE special publications (Warrendale, Pennsylvania), *Magnesium in Automotive Components*, 1996, 1163.
24. Reddy, A. S., Pramila Bai, B. N., Murthy, K. S. and Biswas, S. K., Wear and seizure of binary Al–Si alloys. *Wear*, 1994, **171**, 115–126.
25. Guden, M. and Hall, I. W., High strain-rate compression testing of a short-fiber reinforced aluminum composite. *Mater. Sci. Eng. A*, 1997, **232**, 1–10.
26. Srivatsan, T. S., Wei, Li and Chang, C. F., The tensile behavior of rapidly solidified magnesium alloys. *J. Mat. Sci.*, 1995, **30**, 1832–1838.
27. Jayamathy, M., Structure–property studies on magnesium-based metal matrix composites. Master of Science Thesis, Department of Mechanical Engineering, Indian Institute of Science, Bangalore, December 2001.

ACKNOWLEDGEMENTS. We thank the unknown reviewers for the time, effort, patience and comments, which have helped in strengthening the technical acumen of the manuscript.

Received 3 April 2004; revised accepted 16 June 2004